Core-level spectroscopy calculation and the plane wave pseudopotential method

2009 J. Phys.: Condens. Matter 21 104203

(http://iopscience.iop.org/0953-8984/21/10/104203)

J. Phys.: Condens. Matter **21** (2009) 104203 (12pp) doi:10.1088/0953-8984/21/10/104203

Core-level spectroscopy calculation and the plane wave pseudopotential method

Shang-Peng Gao[1], Chris J Pickard[2], Alexander Perlov[3] and Victor Milman[3]

[1] Department of Materials Science, Fudan University, Shanghai 200433, People's Republic of China
[2] School of Physics and Astronomy, University of St Andrews, St Andrews KY16 9SS, UK
[3] Accelrys, 334 Science Park, Cambridge CB4 0WN, UK

E-mail: cjp10@st-andrews.ac.uk

Received 15 September 2008, in final form 14 October 2008
Published 10 February 2009
Online at stacks.iop.org/JPhysCM/21/104203

Abstract
A plane wave based method for the calculation of core-level spectra is presented. We provide details of the implementation of the method in the pseudopotential density functional code CASTEP, including technical issues concerning the calculations, and discuss the applicability and accuracy of the method. A number of examples are provided for comparing the results to both experiment and other density functional theory techniques.

(Some figures in this article are in colour only in the electronic version)

1. Introduction

Spectroscopic techniques that explore transitions from or to core-level orbitals, such as core-loss electron energy-loss spectroscopy (EELS), x-ray absorption spectroscopy (XAS), x-ray emission spectroscopy (XES), and inelastic x-ray scattering (IXS), have provided a large variety of experimental probes to investigate properties of materials, nanostructures, and biological molecules. There are several versions of EELS, and among them EELS associated with electron microscopy has been a popular tool for material characterization [1]. Third generation synchrotron facilities offer better x-ray sources, and most of them offer beam lines for XAS and IXS. Now there are thirteen third generation synchrotron radiation facilities across the world and another twelve are under construction. This will further promote the use of core-level spectroscopy in materials science. Theoretical calculations based on density functional theory (DFT) [2–5], time-dependent DFT [6, 7], or many-body perturbation theory [8, 9] offer a complementary tool to the experimental core-level spectroscopy.

The plane wave pseudopotential method [10] is the dominant electronic structure method in materials science and condensed matter physics and it is also widely used in chemistry community. It offers an excellent balance of accuracy and computational efficiency [10]. However, it has not been used as widely in core-level spectroscopy calculation as all-electron electronic structure techniques. There are two apparent problems with core-level spectroscopy calculation within the plane wave pseudopotential method: the matrix element calculation and the incorporation of the core–hole effect. It is not entirely straightforward in a pseudopotential code to evaluate the core-excited matrix element, as the valence and conduction band wavefunctions which are optimized in a plane wave pseudopotential code are pseudowavefunctions. It only matches the 'real' wavefunction outside the core region, but the transition which is dominated by the core region is very important for core-level spectroscopy. In an all-electron method, a conventional way to include the core–hole effect is to remove one electron from core orbitals. However, the core orbital is not explicitly included in a pseudopotential calculation.

The site- and angular-momentum-projected density-of-states of the final states of the excited electron has been a natural approximation to the core-level spectra, especially for the K-edge which is due to excitations from the 1s orbital. In the plane wave pseudopotential method, the projected density of states (PDOS) is obtained by projecting the pseudowavefunction onto the pseudoatomic partial waves with required symmetry, i.e. p for transition from the core orbital with s symmetry. Köstlmeier and Elsässer have used this approach to calculate both anion and cation ELNES of metal oxides, and they have given a detailed discussion of the efficiency and the limitations of the method [11, 12]. Gao *et al*

calculated K-edges in a number of materials including group-III nitrides [13], carbon and boron nitride polymorphs [14], and CaB_6 [15]. In these studies, a small cutoff radius in PDOS projection was employed. Good agreement with experiments has been achieved and theoretical core-level spectra were used successfully in interpreting experimental spectra, predicating theoretical reference spectra when reliable experimental spectra were not available, identifying correlations between EELS spectra and crystal structure, and estimating the reliability of experimental spectra [16]. The success of this approach has two reasons: the core–hole effect is taken into account by specially constructed pseudopotential and supercell approximation, and the main matrix element effects are mimicked by PDOS and small cutoff radius when doing the projection. However, explicit evaluation of matrix elements is important for general cases, such as $L_{2,3}$ edge, and the pseudopotential error should be given more careful treatment when applied to wide range of systems. Finally, an absolute value of inelastic cross section is of interest in some cases.

The theory of EELS within plane wave pseudopotential method has been developed by Pickard *et al* [3, 17, 18], and the calculated K-edge spectra of diamond and cubic boron nitride have been shown to agree well with experimental measurements [19]. Subsequently, Pickard developed on-the-fly generation of ultrasoft pseudopotentials within CASTEP [20, 21], a widely used plane wave pseudopotential code. This made it possible to straightforwardly generate an excited pseudopotential, which is required in order to enable the inclusion of the core–hole effect by non-expert users. In the present article we will describe the theory behind core-level spectroscopy calculations and an implementation in the current version of CASTEP. In our approach both the advantages of the pseudopotential method, i.e., reduced computational cost and the ability to study very large systems, and the accuracy of all-electron methods are retained. A description of the implemented method and technical details are given in section 2, and in section 3 we present atomic and solid state tests results of PAW reconstruction and show that results obtained from our approach are equivalent to that from all-electron calculation. The effectiveness of pseudopotential error correction and the role of different terms in the formulation are also discussed. Example applications are presented in section 4, followed by conclusions in section 5.

2. Theory and implementation within the CASTEP code

For the calculation of core-level spectroscopy, the key step is the evaluation of the transition matrix elements $\langle\phi_c|\hat{O}|\psi_{n,k}\rangle$ between the core state $|\phi_c\rangle$ on the site of interest and the unoccupied final state $|\psi_{n,k}\rangle$. The core state $|\phi_c\rangle$ can be obtained from an atomic all-electron calculation. According to the projector augmented wave (PAW) approach [22], an all-electron wavefunction $|\psi_{n,k}\rangle$ can be recovered from the corresponding pseudowavefunction $|\tilde{\psi}_{n,k}\rangle$ via a linear transformation. The transition matrix element can be calculated by:

$$\langle\phi_c|\hat{O}|\psi_{n,k}\rangle = \langle\phi_c|\hat{O}|\tilde{\psi}_{n,k}\rangle + \sum_i \left(\langle\phi_c|\hat{O}|\phi_i\rangle - \langle\phi_c|\hat{O}|\tilde{\phi}_i\rangle\right)\left\langle\tilde{p}_i|\tilde{\psi}_{n,k}\right\rangle \quad (1)$$

where ϕ_i and $\tilde{\phi}_i$ are all-electron and pseudo partial waves respectively. $\tilde{p}_i$ is the PAW projector function localized within the augmentation region and it obeys the relation $\langle\tilde{p}_i|\tilde{\phi}_j\rangle = \delta_{ij}$. Two projectors are constructed for each angular momentum for the ultrasoft pseudopotentials used in our calculations.

The operator $\hat{O}$ for core-loss EELS is

$$\hat{O}_E = \exp(i\vec{q}\cdot\vec{r}) = 1 + i\vec{q}\cdot\vec{r} + \cdots \quad (2)$$

where $\vec{q}$ is the scattering vector or momentum transfer of the incident electron and $\vec{r}$ is the position of the excited electron. The leading term has no contribution to the matrix element because the initial and final states are orthogonal. The dipole approximation is obtained when $\vec{q}\cdot\vec{r}$ is much smaller than 1, that is justified for most transmission EELS experiments, particularly when a small axial collection aperture is employed [1]. For x-ray absorption spectroscopy, the operator $\hat{O}$ can be written as

$$\hat{O}_X = \exp[i(\omega/c)\hat{n}\cdot\vec{r}]\hat{\varepsilon}\cdot\vec{p} \quad (3)$$

where $\hat{\varepsilon}$ and $\hat{n}$ are unit vectors which specify the direction of polarization and the direction of propagation, respectively. $\vec{p}$ is the momentum operator. When the wavelength of the x-ray which induces the transitions is much larger than the extent of the core orbitals, the electric dipole approximation applies.

The transition matrix element of core-loss EELS or XAS within the dipole approximation can be written as

$$\langle\phi_c|r_\alpha\left|\psi_{n,k}\right\rangle = \langle\phi_c|r_\alpha\left|\tilde{\psi}_{n,k}\right\rangle + \sum_i \left(\langle\phi_c|r_\alpha|\phi_i\rangle - \langle\phi_c|r_\alpha\left|\tilde{\phi}_i\right\rangle\right)\left\langle\tilde{p}_i|\tilde{\psi}_{n,k}\right\rangle \quad (4)$$

where $r_\alpha = x, y, z$. The uncorrected term $\langle\phi_c|r_\alpha|\tilde{\psi}_{n,k}\rangle$ is the dipole matrix element between core orbital and the pseudowavefunction. And we want to stress that although $|\phi_c\rangle$ has high frequency components which are not included in the plane wave basis, but the corresponding elements for $|\tilde{\psi}_{n,k}\rangle$ are zero. $(\langle\phi_c|r_\alpha|\phi_i\rangle - \langle\phi_c|r_\alpha|\tilde{\phi}_i\rangle)$ can be evaluated once in real space for each pseudopotential used.

An example of the input.cell file in CASTEP calculation of Al $L_{2,3}$ edge of wurtzite AlN can be found in appendix. There are 16 Al atoms in the $2 \times 2 \times 2$ supercell, and we chose one of them as the 'excited' atom where the core hole localized and labelled it as Al:exi. The pseudopotential for Al:exi can be generated on the fly by writing an appropriate definition string. The {2p5.00, 3p2.00} notation in the string indicates that the atomic configuration is adjusted to model the 2p core hole. Materials Studio graphical user interface [23] provides an automated way of generating the definition of such 'excited' pseudopotential.

3. Test calculations and discussion

We have carried out calculation for both free atoms and crystals to validate and test the accuracy of the PAW reconstruction

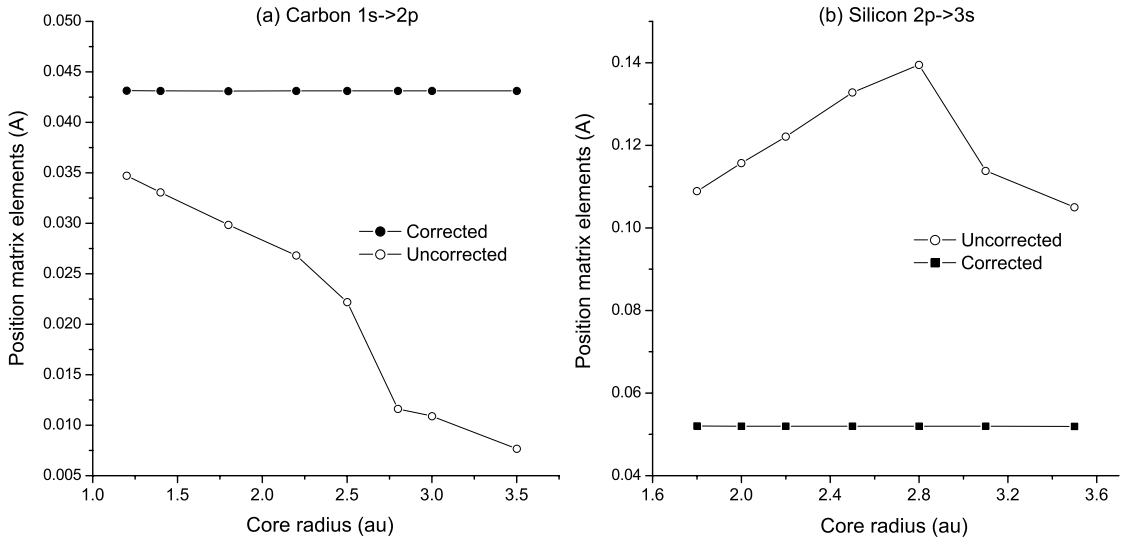

Figure 1. Atomic dipole matrix elements calculated with and without PAW correction. The CASTEP calculations are performed using a FCC cell of 14.14 Å to model the isolated atom. Atomic dipole matrix elements (a) from 1s to 2p in carbon and (b) from 2p to 3s in silicon are plotted versus the core radius employed in the pseudopotential generation.

Table 1. Comparison between atomic dipole matrix elements of carbon, silicon, and gallium calculated using (i) plane waves and pseudopotentials, (ii) all-electron methods.

	CASTEP		
	Uncorrected	PAW corrected	All-electron
Carbon			
$1s \rightarrow 2p$	3.306×10^{-2}	4.313×10^{-2}	4.313×10^{-2}
Silicon			
$1s \rightarrow 3p$	7.135×10^{-4}	4.585×10^{-3}	4.585×10^{-3}
$2s \rightarrow 3p$	6.267×10^{-2}	3.032×10^{-2}	3.032×10^{-2}
$2p \rightarrow 3s$	0.1089	5.021×10^{-2}	5.198×10^{-2}
Gallium			
$1s \rightarrow 4p$	1.292×10^{-5}	6.135×10^{-4}	6.133×10^{-4}
$2s \rightarrow 4p$	1.132×10^{-3}	3.692×10^{-3}	3.696×10^{-3}
$2p \rightarrow 4s$	3.646×10^{-3}	2.992×10^{-3}	2.997×10^{-3}
$2p \rightarrow 4d$	3.033×10^{-3}	4.949×10^{-2}	4.951×10^{-2}

approach in our implementation. Tests of isolated carbon, silicon, and gallium atoms are shown in table 1. The uncorrected matrix elements in table 1 are the position matrix element between core orbital and pseudowavefunction of final states, i.e. the first term in the right-hand side of equation (4). The PAW corrected matrix elements are obtained via equation (4), i.e. contain contribution from all three terms in the right side of the equation (4). Isolated atoms are modelled by placing a single atom in an FCC cell with the edge of 14.14 Å. The values of matrix elements calculated by plane wave pseudopotential method with PAW reconstruction are nearly identical to those calculated by atomic all-electron real space calculation.

If we change the core radius employed in the pseudopotential generation, the pseudowavefunction will change correspondingly within the core region. The contribution from uncorrected part and PAW part would vary, but their sum should remain unchanged. Figure 1 shows uncorrected and corrected dipole matrix elements from 1s to 2p in carbon and from 2p to 3s in silicon. It clearly shows that although the uncorrected dipole matrix elements vary with the pseudopotential core radius, the matrix element with the pseudopotential error corrected remains constant.

Solid state tests for the core-level spectra calculation with and without PAW correction were performed for the carbon K-edge in diamond and L_3-edge in silicon crystal. The uncorrected and corrected spectra for carbon are shown in figure 2 and for silicon in figure 3. It can be seen in figure 2(a) that the uncorrected carbon K-edge calculated using a pseudopotential with the 1.2 au core radius is slightly larger than that using pseudopotential with the 1.4 au core radius. After PAW reconstruction, they gave essentially the same spectra, as shown in figure 2(b). Similar result of PAW reconstruction can be found for silicon L_3-edge which relates to a more complicated excitation processes and contains the transition from 2p to final states with both s and d symmetries. Comparison between experimental and theoretical spectra for a series of materials can be found in [4] and more examples are shown in section 4.

The first term $\langle\phi_c|r_\alpha|\tilde{\psi}_{n,k}\rangle$ and third term $-\sum_i \langle\phi_c|r_\alpha|\tilde{\phi}_i\rangle \langle\tilde{p}_i|\tilde{\psi}_{n,k}\rangle$ in the right-hand side of equation (4) may approximately cancel when the core wavefunction is localized on the site of the excited atom. Taillefumier *et al* [24] used only the second term $\sum_i \langle\phi_c|r_\alpha|\phi_i\rangle\langle\tilde{p}_i|\tilde{\psi}_{n,k}\rangle$ and then applied the recursion method to avoid calculating unoccupied states explicitly. However, in a real system, the core wavefunctions are not strictly localized and have a tail beyond the core region. The approximation should be more accurate for 1s core states than for 2p. We have carried out ground state calculation for core-level spectra from carbon 1s core orbital of graphite and Si $2p_x$ core orbital of cubic silicon carbide. The results are shown in figure 4. Dashed lines correspond to the second term in the right-hand side of equation (4), and solid lines correspond to full terms in the right-hand side of equation (4). We can see that the approximation is quite good for carbon K-edge although slight discrepancy still can be found in the energy range near the threshold. For the transition from $2p_x$ core

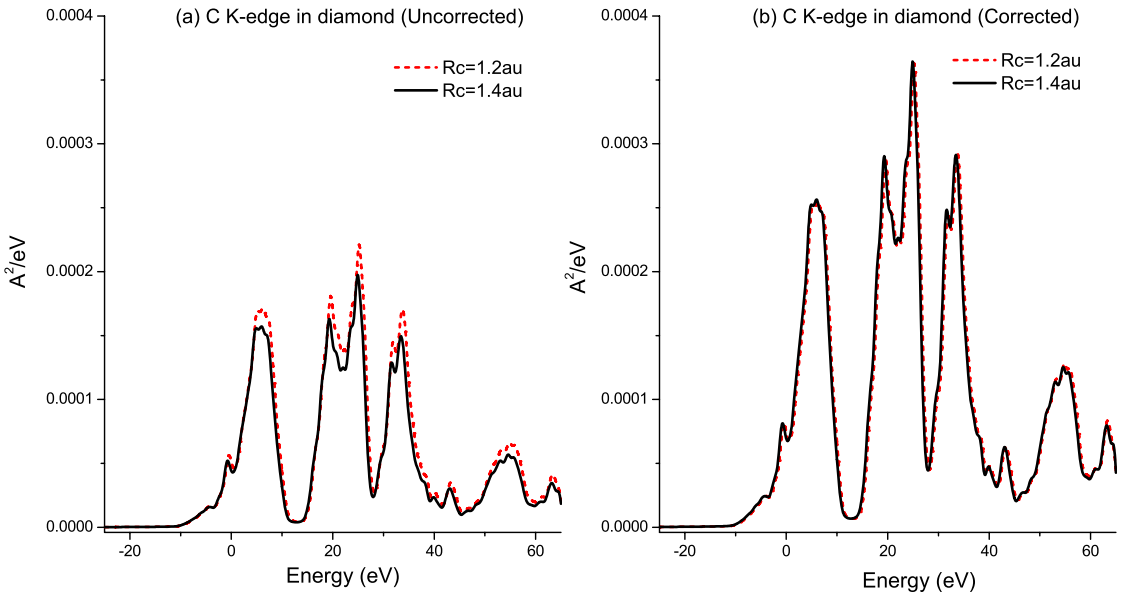

Figure 2. Ground state calculation for C K-edge in diamond (a) with PAW correction and (b) without PAW correction. The results using carbon pseudopotential with core radius 1.2 and 1.4 au are presented together for comparison.

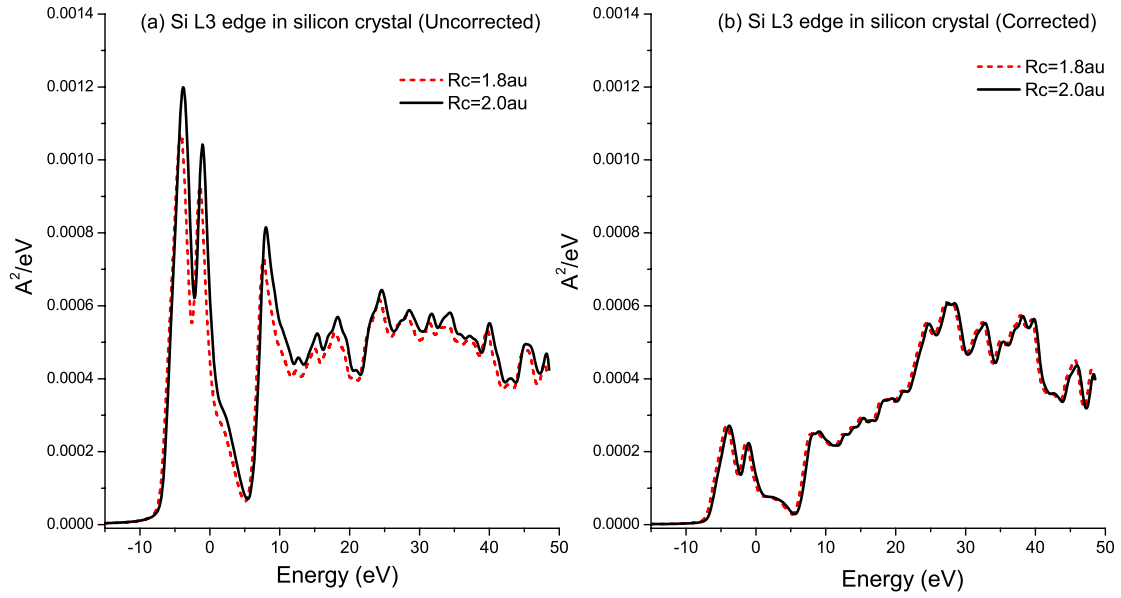

Figure 3. Ground state calculation for Si L_3-edge in silicon crystal (a) with PAW correction and (b) without PAW correction. The results using silicon pseudopotential with core radius of 1.8 and 2.0 au are presented together for comparison.

orbital of silicon, the discrepancy between the spectra is quite obvious. Figure 5 shows the energy dependence of the ratio between the full terms and the second term. The approximation works better for higher energies in both cases. In our method, $\langle\phi_c|r_\alpha|\tilde{\psi}_{n,k}\rangle$ is actually no harder to calculate than $\langle\tilde{p}_i|\tilde{\psi}_{n,k}\rangle$, so full terms of PAW reconstruction are always used.

4. CASTEP ELNES applications

The CASTEP implementation of core-level spectroscopy is sufficiently new to warrant extensive testing against the existing body of experimental and theoretical studies of ELNES in various materials. There is no doubt that DFT itself is capable of accurate description of core-loss spectra. As an example of the wide range of successful DFT applications one could quote a list of publications that used TELNES code in the WIEN2k package to investigate core-loss spectra [25]. This list includes numerous calculations of K- and L-edge spectra of various elements in both simple and complex structures. There remains an open question though of the accuracy of pseudopotential description of the processes which by definition refer to core electrons. CASTEP pseudopotential methodology has been already tested on some model systems [4]. The results presented in this paper further

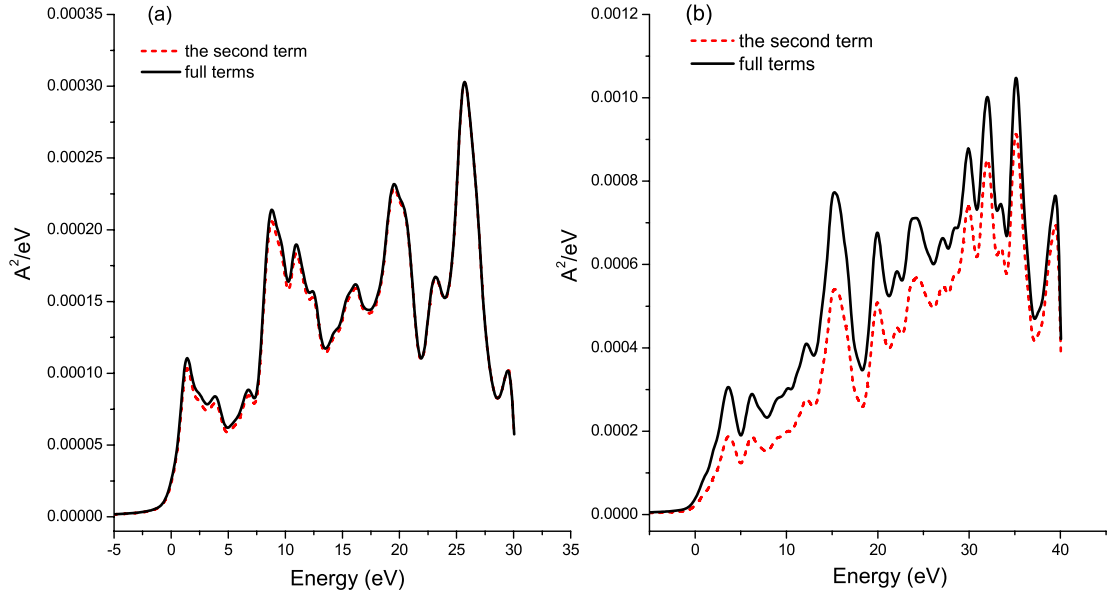

Figure 4. A ground state test calculation for core-level spectra (a) excited from C 1s in graphite (only plot out the first equivalent atom) and (b) excited from Si $2p_x$ in cubic SiC to verify the cancellation between $\langle\phi_c|r_\alpha|\tilde{\psi}_{n,k}\rangle$ and $-\sum_i \langle\phi_c|r_\alpha|\tilde{\phi}_i\rangle\langle\tilde{p}_i|\tilde{\psi}_{n,k}\rangle$ terms adopted from [24]. Dashed lines represent results corresponding to the $\sum_i \langle\phi_c|r_\alpha|\phi_i\rangle\langle\tilde{p}_i|\tilde{\psi}_{n,k}\rangle$ term and solid lines represent results obtained from full terms.

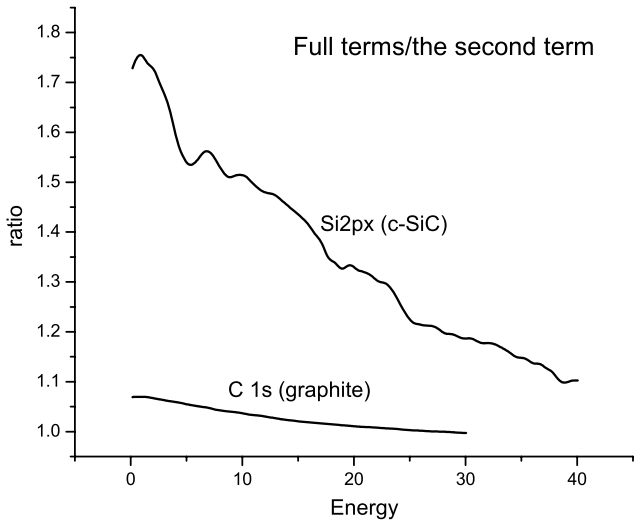

Figure 5. Energy-dependent ratio between spectra calculated from the full terms and from the second term of figure 4.

enhance the body of data available for comparison between CASTEP, WIEN2k and experimental results. In addition we applied CASTEP calculations to interpret recent experimental data [26] on O K-edge ELNES spectra of complex phosphate structures. These systems have not been analysed from first principles before, and first principles analysis is required to explain the difference in fingerprints of two materials studied.

All calculations presented below are carried out using CASTEP code [20]. CASTEP uses plane wave basis set and pseudopotentials within the density functional theory formalism. PBE version of the generalized gradient approximation (GGA) [27] was used to describe exchange–correlation functional. Ultrasoft pseudopotentials were generated on the fly, and one core electron was removed from a relevant core level when performing core–hole calculations. We present also some results obtained without a core hole to illustrate importance of taking the hole into account. All core–hole calculations were carried out using supercells sufficiently large to eliminate unphysical interactions between periodic images. Previous experience from all-electron calculations gives 8–10 Å as a recommended distance between images.

Crystal symmetry is reduced when a core hole is introduced in a supercell. All calculations were carried out by using reduced symmetry rather than by ignoring point group symmetry altogether; even a reduced symmetry allows to speed up calculations by considering only k-points in the irreducible part of the Brillouin zone.

The spectra presented below are adjusted so that the zero energy corresponds to the edge energy. It is possible to determine the absolute values of the edge in a pseudopotential calculation by comparing total energies of systems with and without a core-hole excitation and taking into account a correction term from the contribution of the core orbitals [28]. We have not used this approach in the present study. Simple Gaussian smearing was applied to mimic experimental spectra; typical broadening widths were 0.4–0.6 eV. The theory of ELNES broadening is complicated, various terms corresponding to the lifetime of the core hole, the lifetime of the excited state, and instrumental broadening should be considered [25]. The main result of taking into account all of these effects is that one has to apply a complex function with the energy-dependent broadening factor in order to compare calculated spectra to experimental ones. We ignore this procedure which essentially means that CASTEP results contain sharper features at high energies above the threshold than experimental measurements are capable of resolving.

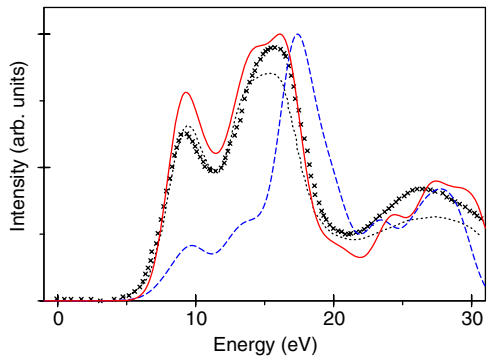

Figure 6. Mg K-edge in MgO: comparison of calculated CASTEP results (present work) to WIEN2k calculations and experimental spectra. Atom with a core hole, CASTEP (solid line); the same, WIEN2k (short dashed line, [29]); atom without a core hole, CASTEP (dashed line); experiment, crosses [29].

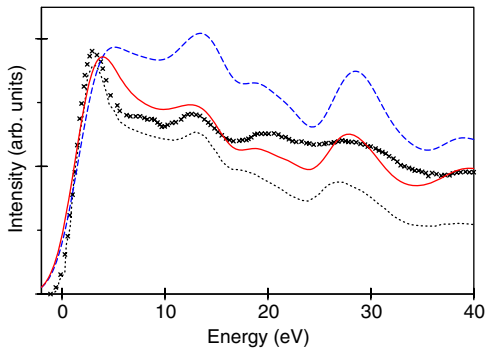

Figure 7. Si K-edge in pure silicon: comparison of calculated CASTEP results (present work) to WIEN2k calculations and experimental spectra. Atom with a core hole, CASTEP (solid line); the same, WIEN2k (dotted line, [29]); atom without a core hole, CASTEP (dashed line); experiment, crosses [29].

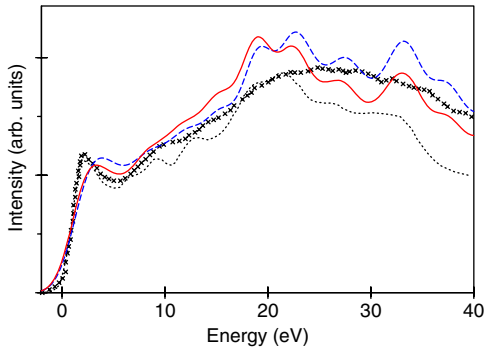

Figure 8. Si $L_{2,3}$ edge in pure silicon: comparison of calculated CASTEP results (present work) to WIEN2k calculations and experimental spectra. Atom with a core hole, CASTEP (solid line); the same, WIEN2k (dotted line [29]); atom without a core hole, CASTEP (dashed line); experiment, crosses [29].

CASTEP calculations do not include spin–orbit interaction and are thus not capable to distinguish between $p_{1/2}$ and $p_{3/2}$ core states. The results we obtain are thus labelled as simply $L_{2,3}$ edge and they are compared to experimental L_2 data.

4.1. Mg K-edge in magnesium oxide

MgO has been shown to be a prime example of a material where an introduction of a core hole is necessary to describe experimental results adequately [29]. CASTEP core-hole calculations were performed using a $2 \times 2 \times 2$ supercell which contained 64 atoms. The plane wave basis set was constructed using the energy cutoff of 500 eV, $2 \times 2 \times 2$ Monkhorst–Pack set of k-points was used for Brillouin zone sampling. Figure 6 shows the comparison of Mg K-edge spectra calculated using CASTEP for an atom with a core hole and an atom without a hole. We also show experimental data and published all-electron results [29]. The broadening of 0.6 eV was applied to CASTEP spectra. It is clear from the comparison that pseudopotential results agree with experiment at least as well as all-electron ones. We also see the same effect due to the core hole as was observed in the WIEN2k calculations [29]: the intensity of the low energy peaks is dramatically underestimated if the excitation is not included explicitly in the calculation.

4.2. Silicon K- and L-edge

Silicon ELNES has been extensively studied both experimentally and theoretically [29]. Present calculation uses $2 \times 2 \times 2$ supercell with 64 atoms, 150 eV energy cutoff, and a $2 \times 2 \times 2$ Monkhorst–Pack k-points set. We carried out separate calculations with 1s and 2p core holes to investigate K and L ELNES spectra. Figures 7 and 8 show the results for Si K-edge and L-edge spectra, respectively. We compare CASTEP results for an atom with a core hole and an atom without a hole to experimental data and published all-electron results [29]. The broadening of 0.6 eV was applied to CASTEP spectra.

Si K-edge in pure silicon requires the core hole to describe the structure of the low energy part of the spectrum, similar to the MgO case. However, omission of excitation in the calculation for Si still produces fairly accurate peak positions (figure 7), only the relative intensities are completely wrong—Mg spectrum in MgO exhibits wrong peak energies as well as intensities.

Pseudopotential results for Si K-edge are very close to the experimental spectrum and are at least as accurate as all-electron WIEN2k calculation (figure 7). Both the relative peak positions and intensities are reliable over the energy range of 40 eV, which is a fairly wide range considering a potential transferability issue inherent in the pseudopotential approximation.

Si L_2 edge results are presented in figure 8. Once again both CASTEP and WIEN2k reproduce experimental results quite well. The role of the core hole is significantly reduced in this case, and it is possible to get a fairly accurate description of the Si $L_{2,3}$ edge spectrum without having to introduce a core hole. The difference in the role played by the core hole for K and $L_{2,3}$ edges is due to the different degree of localization of the states contributing to the transition. K-edge is due to the transition from the valence p-states that are more strongly localized in the crystal than valence s-states responsible for the $L_{2,3}$ spectrum. The effect of a core hole is seen more strongly

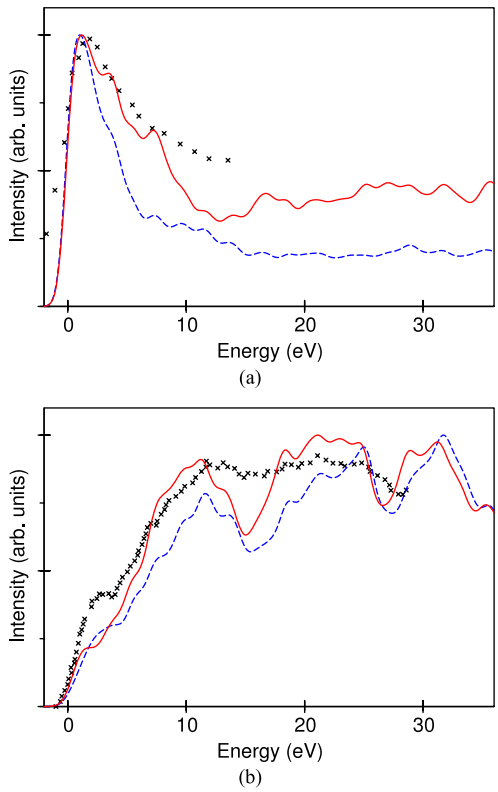

Figure 9. Ni $L_{2,3}$ edge (a) and Si $L_{2,3}$ edge (b) in NiSi. Atom with a core hole, CASTEP (solid line); atom without a core hole, CASTEP (dashed line); experiment, crosses [30].

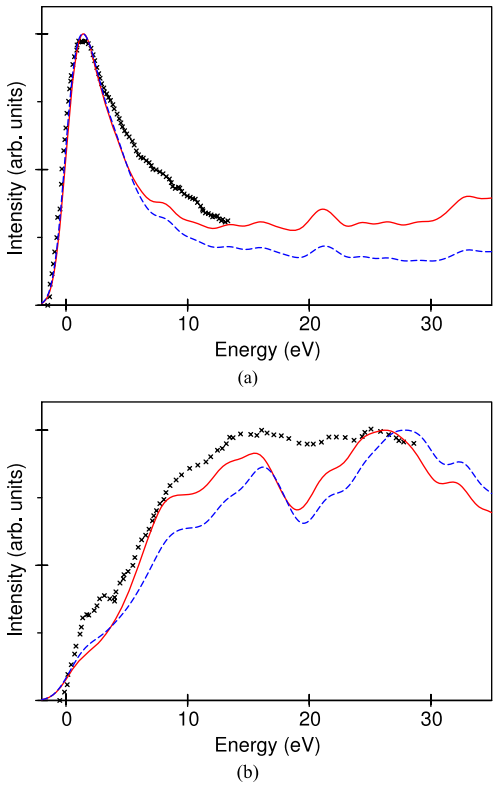

Figure 10. Ni $L_{2,3}$ edge (a) and Si $L_{2,3}$ edge (b) in Ni_2Si. Atom with a core hole, CASTEP (solid line); atom without a core hole, CASTEP (dashed line); experiment, crosses [30].

on localized states, which also explains why the effect is small in good metals with highly delocalized electron distribution.

4.3. $L_{2,3}$ edge in nickel silicides

Experimental and theoretical results for Ni and Si $L_{2,3}$-edge have been reported recently for Ni_2Si and NiSi silicides [30]. These materials are metallic; hence one expects the core hole to be well screened and to have little effect on the observed spectra. Available all-electron calculations with WIEN2k code have been performed without a core hole and using small unit cells.

CASTEP calculations reported below were performed for the orthorhombic NiSi, space group *Pnma* [31]. The structure of the orthorhombic Ni_2Si, space group *Pbnm*, was taken from [32]. We used a $2 \times 3 \times 2$ supercell containing 96 atoms for NiSi and a $1 \times 2 \times 2$ supercell with 48 atoms for Ni_2Si. Monkhorst–Pack k-points defined as a $2 \times 3 \times 2$ and $4 \times 3 \times 3$ set were used for NiSi and Ni_2Si, respectively. Core holes were introduced on a single Ni or Si atom, so that every calculation would have at most one core hole in a supercell. The results allow us to judge whether the assumption of a total neglect of core-hole effects can be justified [30]. The broadening width of 0.6 eV was used for all charts.

Figures 9 and 10 show very good agreement of calculated Ni and Si spectra with experiment [30]. The core-hole effect is not pronounced in these silicides, although the introduction of a core hole does change the positions and relative intensities of spectral features somewhat.

4.4. Nitrogen K-edge in TiN

Titanium nitride is a hard refractory material which is used in various industrial applications due to its unique mechanical properties. Electronic structure and mechanical properties of bulk TiN as well as its surface properties have been studied extensively, see e.g. [33]. Nitrogen K-edge spectra were studied experimentally as a way to relate changes in electronic structure to modifications of the crystal structure. Experimental data have been reported in [34] and [35], and a variety of theoretical methods have been applied to calculate these spectra: real space multiple scattering code FEFF8 in [34], all-electron LMTO method in [35], all-electron FLAPW method in [36]. All theoretical techniques provide good description of the experimental spectra, which implies that the hybridization between Ti 3d and N 2p orbitals is reproduced well in the DFT framework.

CASTEP calculations of the N K-edge in TiN were carried out in a $2 \times 2 \times 2$ supercell containing 64 atoms, using 400 eV energy cutoff and a $3 \times 3 \times 3$ Monkhorst–Pack k-points set. Peak positions and main spectral features are reproduced well and agree with available experimental and theoretical results (figure 11). Inclusion of the core hole further improves description of the first peak and of the relative intensities of the first two peaks. The effect of nitrogen core hole is qualitatively similar to the LMTO result obtained in the Slater transition state approximation (self-consistent calculation in the presence of half a core hole) [35].

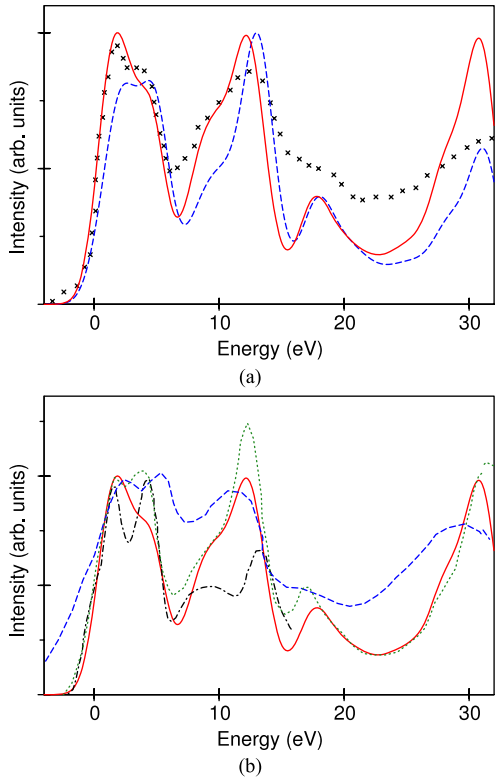

Figure 11. N K-edge in TiN: (a) CASTEP results with core hole (solid line) and without core hole (dashed line) are compared to experimental spectra, crosses [34]; (b) CASTEP results with core hole, solid line, compared to FLAPW WIEN97 results [36], dotted line; FEFF8 results [34], dashed line; LMTO results in Slater transition state approximation [35], dash–dotted line.

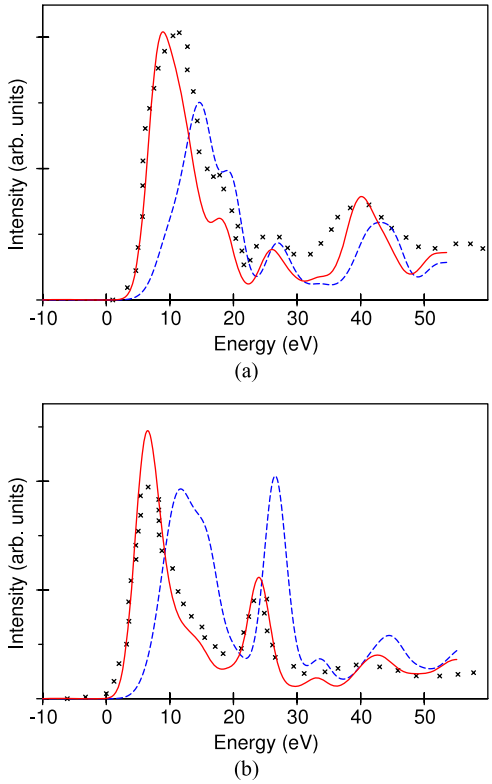

Figure 12. N K-edge (a) and B K-edge (b) in cubic BN: comparison of calculated CASTEP results (core hole, solid line; no core hole, dashed line) to experimental ELNES spectra, crosses [38].

Figure 11(b) shows that CASTEP results are very close to FLAPW from [36], while the spectra from the other two theoretical methods produce slightly different answers. FLAPW can be considered as a reference all-electron DFT result for solid state calculations, and it is thus reassuring to see that pseudopotential approximation in CASTEP does not introduce significant deviations from FLAPW answers.

4.5. B and N K-edge in cubic and hexagonal boron nitride

ELNES spectra for BN have been studied experimentally for a long time. ELNES and XANES results are available for B and N K-edge spectra for cubic BN, see e.g. [37] and [38], and they offer a reliable test system for CASTEP EELS calculations. Results below were obtained from a $3 \times 3 \times 3$ supercell containing 216 atoms. We used the energy cutoff of 400 eV and a $2 \times 2 \times 2$ Monkhorst–Pack set of k-points. Separate calculations were carried out on supercells containing one core hole on B and N atoms, respectively. The results are presented in figure 12 in comparison with ELNES experimental data.

Pseudopotential results describe well the position and relative intensities of the four spectral features in the range of 0–50 eV above the threshold. The core-hole effect is pronounced in this system as can be seen most clearly from the B K-edge, see figure 12(b). Calculations without the core hole produce energy shift of the spectra by 5–7 eV towards higher energies, and fail to reproduce the 2:1 ratio of intensities of the two main peaks. Agreement with experiment is at least as good as in a real space multiple scattering calculation in $Z + 1$ approximation which simulates the core-hole effect [37].

Generally, an EELS experiment is sensitive to the relative orientation of the sample with respect to the beam, and experiments on low symmetry materials show strong orientation dependence of the spectra. The results for hexagonal BN are given below as an example.

Hexagonal boron nitride has been extensively studied [37–40] and presents a useful test system to study the effect of orientation on EELS spectra. CASTEP calculations for h-BN were performed using $3 \times 3 \times 2$ supercells containing 72 atoms. We used the energy cutoff of 400 eV and a $4 \times 4 \times 2$ Monkhorst–Pack set of k-points. Separate calculations were carried out on supercells containing one core hole on B and N atoms, respectively. The results for B and N K-edge spectra are presented in figures 13 and 14.

The main distinctive feature of the comparison between cubic and hexagonal phases of BN is the presence of the strong π^* peak in hexagonal BN when electric field is polarized along the c axis. These peaks in both B and N spectra correspond to transitions from 1s states to the empty π^* states that are related to the planar nature of sp^2 bonded structures. The cubic phase does not have those peaks, and angle-dependent spectra also lack this feature when the polarization of the field is perpendicular to the hexagonal axis. Overall CASTEP calculations describe main spectral features well, provided a

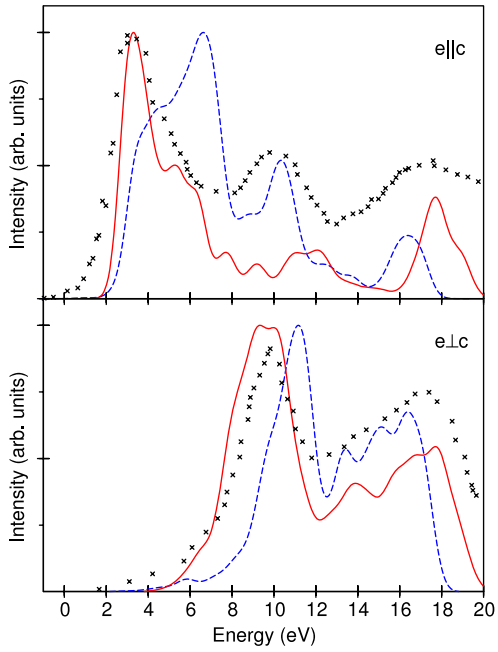

Figure 13. N K-edge in hexagonal BN for electric field polarized along the *c*-axis and perpendicular to it. CASTEP results with core hole (solid line) and without core hole (dashed line) are compared to experimental ELNES data, crosses [39].

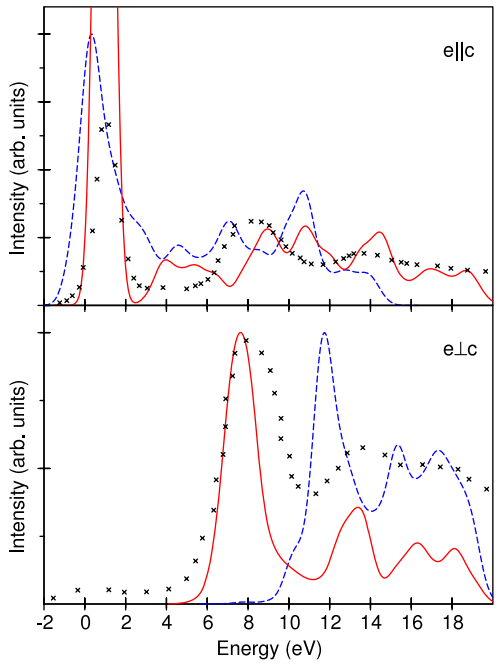

Figure 14. B K-edge in hexagonal BN for electric field polarized along the *c*-axis and perpendicular to it. CASTEP results with core hole (solid line) and without core hole (dashed line) are compared to experimental ELNES, crosses [39].

core hole is included in the calculations. A more detailed description of remaining spectral features and possible reasons for discrepancy between calculations and experiment can be found in [40].

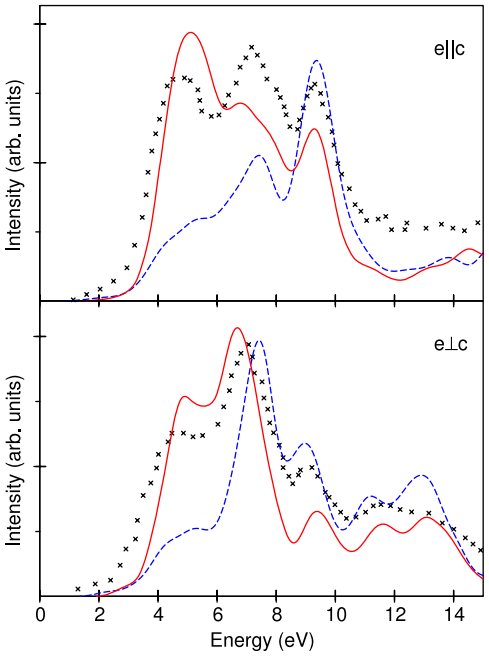

Figure 15. N K-edge in hexagonal GaN for electric field polarized along the *c*-axis and perpendicular to it. CASTEP results with core hole (solid line) and without core hole (dashed line) are compared to experimental ELNES spectra, crosses [41].

4.6. N K-edge in hexagonal GaN

Hexagonal GaN is another anisotropic material where we can compare calculated orientation dependence to available experimental and theoretical data [41, 42]. Calculations in [41] were performed using a real space multiple scattering approach as implemented in the FEFF8 code; the core hole was taken into account by the authors. WIEN2k calculations with core hole of the spectrum for one particular orientation are reported in [42].

CASTEP calculations for h-GaN were performed using a $3\times3\times2$ supercell containing 72 atoms (one nitrogen atom had a core hole). We used the energy cutoff of 400 eV and a $3\times3\times2$ Monkhorst–Pack set of k-points. The results are shown in figure 15 in comparison with experiment. Calculated N K-edge agrees well with the experimental spectrum, especially in terms of the positions of the peaks. Orientation dependence is reproduced well also. FEFF8 calculations reported for this material in [41] provide better description of relative intensities, partly due to the use of a sophisticated energy-dependent broadening function. However, overall quality of the results is very similar and both methods, CASTEP and FEFF8, provide good description of observed features and their orientation dependence.

4.7. O K-edge in hydroxyapatite and β–tricalcium phosphate

The final example refers to the interpretation of the experimental EELS spectra of β-tricalcium phosphate (β-TCP), $Ca_3(PO4)_2$, and hydroxyapatite (HA), $Ca_{10}(PO_4)_6(OH)_2$. These two compounds attract significant attention due to their high potential for bioapplications. A recent study of the EELS

spectra of these compounds [26] was driven by the need to provide an analytical tool to distinguish between these two crystals in composite materials, so-called biphasic calcium phosphates. Experiment suggests that the fine structure of the first peak of the O K-edge spectrum allows one to distinguish between these two compounds: there is a characteristic splitting of the maximum in HA which is absent in pure β-TCP samples.

These phosphates differ from other compounds presented above in that they contain a number of inequivalent positions for the atomic species which is responsible for the signal. Each of these structures contains an arrangement of PO_4 groups; in addition, HA contains disordered columns of OH groups running along the c axis. PO_4 groups in HA are all symmetry equivalent, and each group has three symmetry inequivalent oxygen atoms. β-TCP has a more complex structure with inequivalent PO_4 groups; as a result there are ten different oxygen atoms in the rhombohedral unit cell. Experimental spectra would represent a convolution of signals from all of these atoms.

CASTEP calculations on HA were carried out using the experimental structure [43]. Disordered OH groups in hexagonal HA, space group 176, are oriented along the c axis; CASTEP calculations were performed on a randomly selected configuration of a $1 \times 1 \times 2$ supercell (containing 88 atoms) where some of the OH-group positions were occupied so as to maintain overall stoichiometry, see figure 16(b). We used the energy cutoff of 500 eV and the $2 \times 2 \times 1$ Monkhorst–Pack set of k-points.

The structure of the trigonal β-TCP compound, space group 161, was taken from [44]. Their reported structure contains disordered vacancies on one of the Ca sites; we have ignored this and studied fully ordered β-TCP. CASTEP calculations on this system were performed in the rhombohedral setting for a cell containing 92 atoms. We used 500 eV energy cutoff and the $2 \times 2 \times 2$ k-point set. The broadening width of 0.4 eV was used in all calculations.

The results for HA are showed in figure 16(a). The spectrum from the oxygen in OH groups is completely different from the signal due to oxygen atoms in the PO_4 group. The main peak from the OH oxygen is at much lower energy of only 2 eV, with just a weak feature at 7–8 eV above the edge where the main peak of PO_4 oxygens lies. It is likely that the experimental signal reflects only the PO_4 group, and structural disorder masks any possible signal from the OH groups. Note the overall good description of the spectrum: the splitting of the main peak into two components of roughly the same intensity that are separated by about 1.3 eV, a small feature at about 6 eV above the second hump of the main peak, and a wide shoulder at higher energies.

We used the following procedure when combining calculated spectra from different oxygen atoms. Each spectrum was obtained from a simulation with a core hole on a corresponding atom. We used the differences in total energies from these calculations as a measure of the difference in chemical shifts on oxygen, and thus shifted the energy scale of each spectrum accordingly. Finally, the spectra were added up according to the occupancy of the Wyckoff sites for O1, O2 and O3 atoms (6, 6, and 12, respectively). The spectrum from

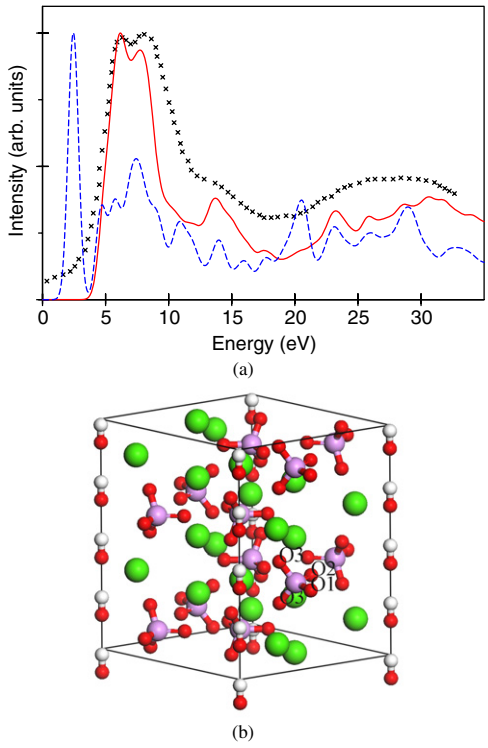

Figure 16. O K-edge in HA (a) and the supercell used in the calculations (b). CASTEP spectra: combined spectrum from PO_4 group (solid line); oxygen from OH groups (dashed line); experimental ELNES data, crosses [26]. Legend: large spheres—Ca, medium spheres—P, small dark spheres—O, small light spheres—H atoms.

OH-group oxygen atoms is shown in figure 16(a) separately—it is obviously different from the spectra of PO_4 group oxygens and bears little resemblance to the experimentally measured one.

β-TCP structure contains ten inequivalent oxygen atoms, see figure 17(b). The overall calculation procedure was similar to that described for HA. Core holes were introduced for each of the ten sites in ten separate calculations. We used the 92 atom cell to generate ELNES spectra for each inequivalent site, and shifted the energy scales according to the calculated total energies. The overall spectrum was obtained by adding up the intensity of individual contributions according to the Wyckoff site symmetry. We also carried out a simpler calculation that did not take the core-hole effect into account (and consequently there was no chemical shift to apply to the individual spectra).

Calculated results are compared to experiment in figure 17(a). There is no splitting of the main peak in agreement with the experimental ELNES spectrum; the main peak is asymmetric and reproduces well the shape of the measured signal. The weaker feature that is about 6–7 eV higher in energy than the main peak is also observed. Both HA and β-TCP exhibit this secondary peak, so it is really the main peak of the O K-edge spectrum that can be used for fingerprinting of these phosphates.

These results question the explanation provided in the experimental study as to the nature of difference in O K-edge spectrum in these two compounds [26]. The initial hypothesis

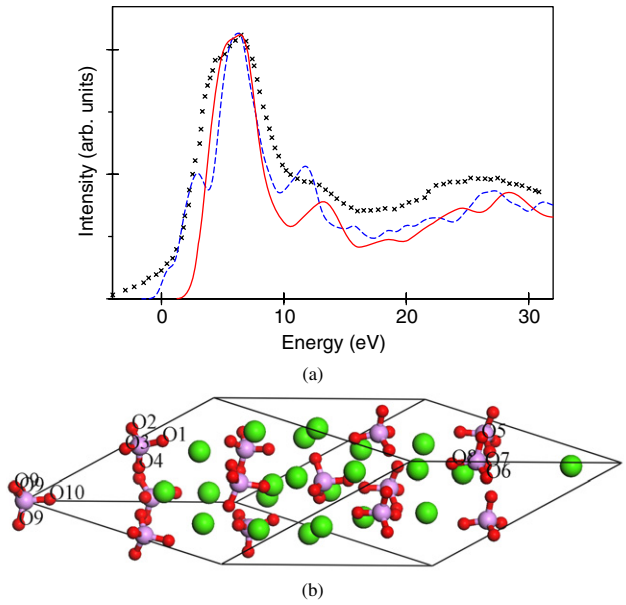

Figure 17. O K-edge in β-TCP (a) and the supercell used in the calculations (b). CASTEP spectrum from all oxygen atoms of the PO_4 groups (with core hole and chemical shifts, solid line; without core hole or chemical shifts, dashed line) is compared to the experimental ELNES data, crosses [26]. Legend: large spheres—Ca, medium spheres—P, small spheres—O.

was that the presence of OH groups and the mixture of signals from OH groups and from PO_4 groups cause the splitting of the main peak in HA. Our results indicate that although the effect is well reproduced in calculations, the underlying reason for the peak splitting is different. Both structures exhibit essentially pure PO_4 signal. The main difference appears to be in the lower symmetry of the β-TCP structure; as a consequence there is a larger spread in possible O geometries in PO_4 groups. The convolution of ten different signals creates an overall smooth peak; in fact, each of the individual peaks has less fine structure as well. This last example shows convincingly that a combination of experimental and theoretical studies can bring out more reliable information about electronic structure and its relation to the crystallographic features than the experimental work alone.

5. Conclusions

Theory, implementation, validation and application of core-level spectroscopy calculation using plane wave pseudopotential method have been presented. Atomic and solid state test results show the importance and success of PAW reconstruction to correct the pseudopotential error in matrix element evaluation. Both the advantage of the pseudopotential method to reduce computational cost and the accuracy of the all-electron method are retained in our approach. Although methodologies based on TDDFT or MBPT can describe core–hole effects in a more rigorous framework and they can give better interpretation for many-body effects related to some specific features, our method can provide good overall agreement with experiments for real systems including large complex low symmetry problems with easily accessed computer resources.

We have showed that in a variety of systems calculated spectra are in good agreement with experiment and with other DFT calculations. Our results were used to interpret for the first time experimental spectra of complex phosphates by explaining the nature of the fingerprint of oxygen K-edge spectra.

Calculations that take core–hole effects into account typically involve supercells containing of the order of 100 atoms which is a perfectly acceptable size for modern computers. It is thus reasonable to expect that this technique will gain further popularity in the near future as a robust and reliable tool for characterization of materials. Further enhancements of the method, such as incorporation of spin–orbit effects, an account of energy-dependent broadening [25], automatic determination of chemical shifts and thus of absolute edge energies [28], and summation of signals of inequivalent atoms would make interpretation of experiments easier. However, this article is an important milestone in that it demonstrates clearly the accuracy and wide applicability of plane waves as a tool for calculation of core-level spectra.

Acknowledgments

We thank Jonathan Yates for helpful discussion. This work is supported by Engineering and Physical Sciences Research Council (UK) and Shanghai Leading Academic Discipline Project, Project Number: B113 (China).

Appendix

An example of the input.cell file in CASTEP calculation of Al $L_{2,3}$ edge of wurtzite AlN is shown below. To save space we did not list all the atom positions in the $2\times2\times2$ supercell which contains 32 atoms and omitted some blocks that are similar to a standard CASTEP calculation.

```
%BLOCK LATTICE_CART
        3.1110000000  -5.3884100000   0.0000000000
        3.1110000000   5.3884100000   0.0000000000
        0.0000000000   0.0000000000   9.9560000000
%ENDBLOCK LATTICE_CART

%BLOCK POSITIONS_FRAC
        Al:exi  0.1666666667  0.3333333333  0.0000000000
        Al   0.6666666667  0.3333333333  0.0000000000
        Al   0.1666666667  0.8333333333  0.0000000000
        ....
        Al   0.8333333333  0.1666666667  0.7500000000
        Al   0.3333333333  0.6666666667  0.7500000000
        Al   0.8333333333  0.6666666667  0.7500000000
        N    0.1666666667  0.3333333333  0.1905000000
        N    0.6666666667  0.3333333333  0.1905000000
        ....
        N    0.3333333333  0.6666666667  0.9405000000
        N    0.8333333333  0.6666666667  0.9405000000
%ENDBLOCK POSITIONS_FRAC
....
%BLOCK SPECIES_POT
         Al  Al_00.usp
          N  N_00.usp
        Al:exi  3|2.0|2.0|1.7|1|2|3|30:31:32{2p5.00,3p2.00}[]
%ENDBLOCK SPECIES_POT
```

The LATTICE_CART block defines the $2 \times 2 \times 2$ supercell, i.e. we have doubled the lattice parameters of the primitive cell.

There are 16 Al atoms in the supercell, and we chose one of them as the 'excited' atom where the core hole localized and labelled it as Al:exi.

References

[1] Egerton R 1996 *Electron Energy Loss Spectroscopy in the Electron Microscope* (New York: Plenum)
[2] Hébert-Souche C, Louf P H, Blaha P, Nelhiebel M, Luitz J, Schattschneider P, Schwarz K and Jouffrey B 2000 *Ultramicroscopy* **83** 9–16
[3] Pickard C J and Payne M C 1997 *Electron. Microsc. Anal.* **153** 179–82
[4] Gao S P, Pickard C J, Payne M C, Zhu J and Yuan J 2008 *Phys. Rev.* B **77** 115122
[5] Mo S-D and Ching W Y 2000 *Phys. Rev.* B **62** 7901
[6] Rehr J J and Ankudinov A L 2003 *Int. J. Quantum Chem.* **95** 487–92
[7] Ankudinov A L, Takimoto Y and Rehr J J 2005 *Phys. Rev.* B **71** 165110–8
[8] Shirley E L 1998 *Phys. Rev. Lett.* **80** 794
[9] Soininen J A and Shirley E L 2001 *Phys. Rev.* B **64** 165112
[10] Payne M C, Teter M P, Allan D C, Arias T A and Joannopoulos J D 1992 *Rev. Mod. Phys.* **64** 1045
[11] Köstlmeier S and Elsässer C 1999 *Phys. Rev.* B **60** 14025
[12] Elsässer C and Köstlmeier S 2001 *Ultramicroscopy* **86** 325–37
[13] Gao S-P, Zhang A, Zhu J and Yuan J 2004 *Appl. Phys. Lett.* **84** 2784–6
[14] Gao S-P, Zhu J and Yuan J 2004 *Chem. Phys. Lett.* **400** 413–8
[15] Gao S-P, Jiang J, Cao M, Zhu J and Yuan J 2004 *Phys. Rev.* B **69** 214419
[16] Zhu J, Gao S-P, Zhang A-H and Yuan J 2005 *J. Electron Microsc.* **54** 293–8
[17] Pickard C J 1997 *PhD Thesis* University of Cambridge
[18] Rez P, Alvarez J R and Pickard C 1999 *Ultramicroscopy* **78** 175–83
[19] Jayawardane D N, Pickard C J, Brown L M and Payne M C 2001 *Phys. Rev.* B **64** 115107
[20] Segall M D, Philip J D L, Probert M J, Pickard C J, Hasnip P J, Clark S J and Payne M C 2002 *J. Phys.: Condens. Matter* **14** 2957–73
[21] Clark S J, Segall M D, Pickard C J, Hasnip P J, Probert M I J, Refson K and Payne M C 2005 *Z. Kristallogr.* **220** 567–70
[22] Blöchl P E 1994 *Phys. Rev.* B **50** 17953
[23] Accelrys 2008 *Materials Studio* 4.4
[24] Taillefumier M, Cabaret D, Flank A-M and Mauri F 2002 *Phys. Rev.* B **66** 195107
[25] Hébert C 2007 *Micron* **38** 12–28
[26] Gregori G, Kleebe H-J, Mayra H and Ziegler G 2006 *J. Eur. Ceram. Soc.* **26** 1473–9
[27] Perdew J P, Burke K and Ernzerhof M 1996 *Phys. Rev. Lett.* **77** 3865–8
[28] Mizoguchi T, Tanaka I, Gao S and Pickard C J 2008 *J. Phys.: Condens. Matter* submitted
[29] Hébert C, Luitz J and Schattschneider P 2003 *Micron* **34** 7
[30] Kawasaki N, Sugiyama N, Otsuka Y, Hashimoto H, Tsujimoto M, Kurata H and Isoda S 2008 *Ultramicroscopy* **108** 399–406
[31] Rabadanov M K and Ataev M B 2002 *Crystallogr. Rep.* **47** 33–8
[32] Wyckoff R W G 1963 *Crystal Structures* (New York: Interscience) pp 298–306
[33] Marlo M and Milman V 2000 *Phys. Rev.* B **62** 2899–907
[34] Mirguet C, Calmels L and Kihn Y 2006 *Micron* **37** 442–8
[35] Paxton A T, Schilfgaarde M v, MacKenzie M and Craven A J 2000 *J. Phys.: Condens. Matter* **12** 729–50
[36] Scott A J, Brydson R, MacKenzie M and Craven A J 2001 *Phys. Rev.* B **63** 245105
[37] Wibbelt M, Kohl H and Kohler-Redlich P 1999 *Phys. Rev.* B **59** 11739–45
[38] Jaouen M, Hug G, Gonnet V, Demazeau G and Tourillon G 1995 *Microsc. Microanal. Microstruct.* **6** 127–39
[39] Arenal R, Kociak M and Zaluzec N J 2007 *Appl. Phys. Lett.* **90** 204105
[40] Moreau P, Boucher F, Goglio G, Foy D, Mauchamp V and Ouvrard G 2006 *Phys. Rev.* B **73** 195111
[41] Moreno M S, Jorissen K and Rehr J J 2007 *Micron* **38** 1–11
[42] Strocov V N, Schmitt T, Rubensson J E, Blaha P, Paskova T and Nilsson P O 2004 *Phys. Status Solidi* b **241** R27–9
[43] de Andrade A V C, da Silva J C Z, Paiva-Santos C O, Weber C, dos Santos Utuni V H, Tebcherani S M, Ferreira Borges C P, da Costa E and Martinez Manent S 2004 Synthesis and crystal phase evaluation of hydroxylapatite using the Rietveld-maximum entropy method *28th Int. Conf. on Advanced Ceramics and Composites B: Ceramics Engineering and Science Proc.* vol 25, ed E Lara-Curzio and M J Ready (New York: Wiley) pp 639–45
[44] Yashima M, Sakai A, Kamiyama T and Hoshikawa A 2003 *J. Solid State Chem.* **175** 272–7